Energy & Buildings 307 (2024) 113922

Contents lists available at ScienceDirect

Energy & Buildings

journal homepage: www.elsevier.com/locate/enb

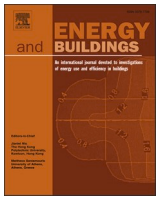

Harnessing the characteristic of compound parabolic concentrators for directional concentration of emitted thermal radiation and solar shielding in building-integrated radiative cooling

Ya Dan, Mingke Hu [1,*], Suhendri Suhendri, Yuehong Su [1], Saffa Riffat

Department of Architecture and Built Environment, University of Nottingham, Nottingham NG7 2RD, UK

ARTICLE INFO

Keywords:
Radiative cooling
Directional atmospheric emissivity
Compound parabolic concentrator
Solar shield
Optical simulation
Experimental study

ABSTRACT

Radiative sky cooling (RC) is a promising solution for meeting the growing cooling demands by passively dissipating waste heat into frigid outer space. However, current RC systems suffer from low cooling power density and limited installation flexibility, impeding their effective application as building cooling strategies. To overcome these challenges, a novel concentrated RC system coupled with a compound parabolic concentrator (CPC) is proposed and experimentally studied. The objective is to investigate the effectiveness of the CPC in enhancing the cooling capability of the RC system and the feasibility of achieving all-day RC in unfavorable working conditions when integrated with building roofs. During nighttime experiments in the humid Nottingham region, the CPC-RC system exhibited an average emitter temperature that was 5.83 °C lower than the ambient temperature, representing a 30 % and 13.6 % improvement in RC performance compared to the flat-RC system and trapezoidal-concentrated RC system, respectively. The Photopia optical software simulation indicates that when the modules are tilted to the north, the CPC functions as a solar shield, effectively limiting solar radiation reaching the emitter surface, which is advantageous for conducting daytime RC experiments. In the daytime experiment, the emitter temperature of the CPC-RC module in anti-sunward group was still 1.59 °C lower than the ambient temperature and 5.49 °C lower than that of flat-RC module. At night, the CPC-RC module of the three placement groups all showed the highest RC effect in the same group. The average emitter temperature of the CPC-RC module in the horizontal placement group is 0.6 °C lower than that of the flat RC module. This novel CPC-RC scheme presents a new energy-saving strategy for buildings and showcases its potential for achieving 24-hour RC when integrated into anti-sunward roofs.

1. Introduction

Global warming, caused by the anthropogenic greenhouse effect, has resulted in frequent heatwaves and extreme weather events [1,2], increasing the risk of overheating for building occupants and amplifying the demand for cooling to meet the thermal comfort of users. Building cooling demand experienced the highest annual growth rate of building sectors through 2021, among nearly 16 % (~2,000TWh) of final electricity consumption in the building industry [3]. Thus, reducing energy consumption for cooling buildings is a crucial global strategic concern. To tackle this challenge, pursuing passive cooling technologies is an urgent and environmentally friendly solution.

Radiative sky cooling (RC) is ubiquitous in daily life and has obtained widespread attention as a promising passive building cooling strategy [4–6]. Unlike conventional vapor compression cooling which creates a local cooling effect at the cost of dumping more heat to the ambient environment through a fossil energy-driven thermodynamic cycle, RC technology is capable of emitting heat to the frigid outer space via the "atmospheric window" (8–13 μm) in an energy- and carbon-free manner, enabling substantial energy savings and environmental protection [7]. However, the cooling efficiency of an RC system is often influenced by the spectral characteristics of the RC emitter surface [8–10] as well as various external factors, including solar intensity [11], relative humidity [12], sky view factor [13], etc. Fig. 1 depicts the heat exchange of an outdoor flat RC emitter. The cooling effect is achieved when the thermal radiation power emitted by the emitter (P_{rad}) exceeds

* Corresponding author.
E-mail address: mingke.hu@nottingham.ac.uk (M. Hu).
[1] The two authors have the same contribution to this study.

https://doi.org/10.1016/j.enbuild.2024.113922
Received 9 September 2023; Received in revised form 20 December 2023; Accepted 17 January 2024
Available online 20 January 2024

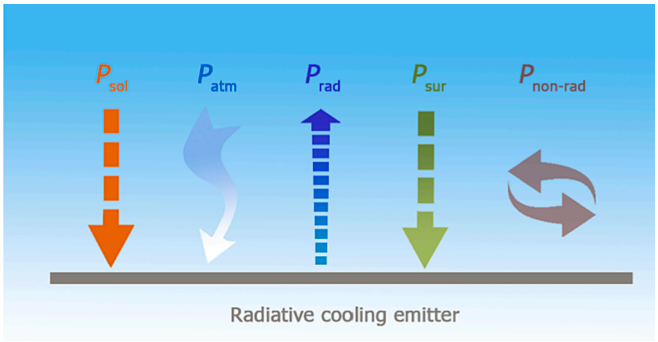

Fig. 1. Schematic of the heat balance of an RC emitter.

the sum of the absorbed solar energy (P_{sol}), atmospheric thermal radiation (P_{atm}), local surrounding thermal radiation (P_{sur}, from nearby buildings, trees, ground, etc.), and incoming non-radiative heat ($P_{non\text{-}rad}$, via heat conduction and convection). Consequently, by decreasing P_{sol}, P_{atm}, P_{sur}, and $P_{non\text{-}rad}$ while increasing P_{rad}, the cooling power of the RC system can be improved.

To increase P_{rad}, the emitter needs to possess a high emissivity throughout the mid- and far-infrared regions (3–50 μm) or at least within the "atmospheric window" to effectively emit thermal radiation into outer space. To minimize $P_{non\text{-}rad}$, using structures such as vacuum boxes, polyethylene (PE) films, and insulating layers can effectively impede the transfer of heat through means other than radiation. Additionally, the emitter should maintain a near-zero absorption within the solar spectrum (0.3–2.5 μm) to reduce P_{sol} [7]. Furthermore, to mitigate P_{atm}, it is beneficial to take advantage of clear skies with lower atmospheric emissivity or to orient the emitter to a smaller zenith angle (with a higher atmospheric transmissivity) [14]. Moreover, installing the system in locations that offer a greater sky view factor can effectively decrease the impact of P_{sur} [13].

In recent decades, there has been a profound exploration of RC driven by significant advancements in materials science and technology. This progress has led to the development of novel RC materials, including metamaterials and polymer-based materials, which exhibit nearly ideal spectral characteristics [15–20], making it quite challenging to improve the RC performance from a material development perspective. Therefore, in terms of enhancing RC power, further research prospects perhaps should lie not so much in material-level advancements but in exploring structural optimization at module and system levels. In this context, concentrated radiative cooling (RC) scheme have emerged as a recent approach to further increase RC power [21]. Concentrated RC systems utilize concentrators (reflectors) to direct and concentrate the hemispherical thermal radiation emitted by RC emitters towards the most transparent region of the sky, typically around the zenith (0° direction), facilitating efficient radiative heat dissipation into deep space [21]. Simultaneously, the concentrators prevent the downward radiation from outside the maximum half-acceptance angle of the concentrators reaching the emitters, effectively reducing the absorption of P_{sol}, P_{atm}, and P_{sur} by the emitter surfaces. Consequently, the cooling effect of the system can be enhanced.

Concentrated RC systems commonly employ concentrators with various structural designs such as parabolic troughs [21,22], inverted pyramids [23], truncated or non-truncated inverted cones [24,25], and V-grooves [26]. In the selection of concentrator materials, aluminum is frequently favored due to its high reflectivity (or low absorption) across both the solar spectrum and infrared region [21,27,28]. Moreover, alternative cost-effective and highly reflective materials, including stainless steel, cermet mirrors [26], and Mylar [24], have exhibited promising potential for concentrator fabrication. Recent physical and mathematical models have substantiated significant enhancements in the cooling efficiency of concentrated RC systems, resulting in a temperature reduction exceeding twofold compared to conventional RC devices lacking concentrators [21].

Before the concentrated RC system was proposed, concentrating technology is widely used in another renewable energy field, concentrated solar energy utilization. This technology employs concentrators to focus a large area of solar irradiance onto a smaller receiver. Among various concentrators, low-concentrators such as the compound parabolic concentrator (CPC) introduced by Winston [29] in 1974, has gained wide practical applications due to their cost-effectiveness and the exemption from requiring additional auxiliary tracking systems. It has been demonstrated that the CPC effectively captures direct solar radiation as well as a portion of scattered radiation when the incident angle is smaller than the half-acceptance angle of the concentrator, consequently improving the concentration efficiency [30–32].

Inspired by existing research on concentrated RC systems and the superior optical efficiency exhibited by CPCs, it is worthwhile to explore the potential of utilizing CPCs as concentrators within concentrated RC systems. Therefore, the present work aims to determine whether incorporating CPCs can further enhance the cooling capacity and address the current limitations associated with integrating RC systems into buildings. In this study, a two-dimensional (2D) CPC-based RC system was developed and fabricated to enhance the RC performance. Outdoor experiments were conducted in Nottingham, UK to measure the emitter temperature of the CPC-based RC module (CPC-RC module) under different conditions, enabling a comprehensive analysis of its cooling performance. Additionally, a series of comparative analyses were performed on the CPC-RC module, a flat-RC module, and another commonly used concentrated RC module, namely the trapezoidal-based RC module (Trapezoidal-RC module).

2. Methodology

To investigate the CPC-RC system and analyze its cooling performance, a standard 2D CPC with a maximum half-acceptance angle of 30° is selected as the concentrator for this study. In Section 2.1, a theoretical analysis is presented aiming to provide a clear understanding of how a CPC-RC system can enhance RC power. Furthermore, Section 2.2 provides a comprehensive description of the experimental setup, covering various aspects such as materials, modules, and the overall system configuration. In Section 2.3, the solar radiation absorbed by CPC-RC module and flat-RC module under direct sunlight is simulated using Photopia, an optical simulation software. Finally, the subjects and objectives of three groups of outdoor experiments are introduced.

2.1. Analysis on directional emitter-sky thermal radiation

In the CPC-RC system, one of the primary functions of the CPC is to concentrate the hemispherical thermal radiation emitted by the emitter towards directions near the zenith to improve cooling performance. Under clear-sky conditions, the spectral, directional atmospheric transmittance $\tau_{atm}(\lambda, \theta)$ can be approximately considered equal to $[1\text{-}\varepsilon_{atm}(\lambda, \theta)]$, in which $\varepsilon_{atm}(\lambda, \theta)$ represents the spectral, directional atmospheric emissivity. The spectral emissivity of the atmosphere at 0° zenith angle can be obtained from C. G. Granqvist and A. Hjortsberg [33], while that of other zenith angles are calculated using the following "box model" equation [33]:

$$\varepsilon_{atm}(\lambda,\theta) = 1 - (\varepsilon_{atm}(\lambda,0))^{1/\cos\theta} \quad (1)$$

Fig. 2(a) shows the spectral atmospheric emissivity at four different zenith angles (0°, 30°, 45° and 60°) within the 0–25 μm wavelength range, while Fig. 2(b) illustrates the weighted average atmospheric emissivity within the "atmospheric window". The weighted average emissivity remains around 0.37 from the zenith direction up to a zenith angle of 40°. However, beyond 50°, the weighted average emissivity increases rapidly, reaching 0.76 at 80°. It can be inferred that as the

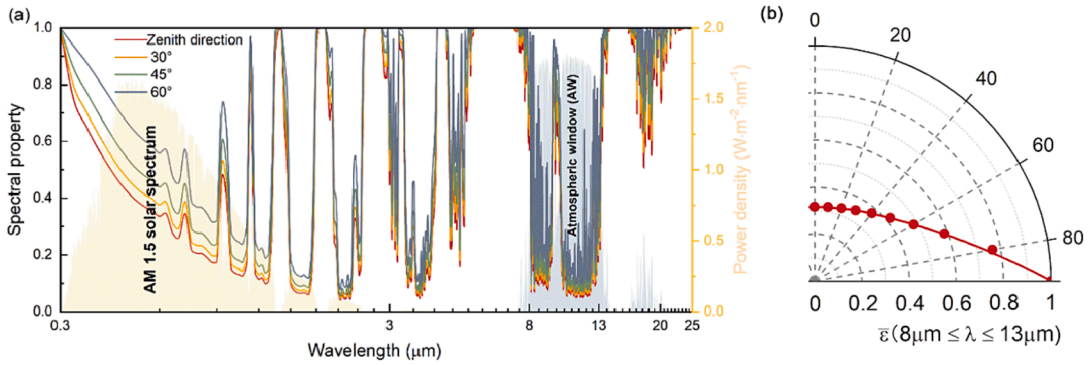

Fig. 2. (a) Spectral atmospheric emissivity of four different zenith angles in the 0.3–25 μm wavelength range. (b) The weighted average atmospheric emissivity between the 8 and 13 μm.

zenith angle increases, resulting in a longer path length of thermal radiation passing through the atmosphere, leading to higher atmospheric emissivity in that direction. Consequently, more thermal radiation emitted by the emitter is absorbed by the atmosphere instead of being emitted into deep space, i.e., the radiation thermal resistance between the emitter and outer space increases, resulting in a decrease in the net RC power in that direction. In contrast, the CPC-RC system effectively reduces the radiation thermal resistance between the emitter and outer space by concentrating the hemispherical thermal radiation within a small zenith angle range (CPC's half-acceptance angle), where the sky is the most transparent.

As shown in Fig. 3(a), the radiation direction of the flat RC emitter is hemispherical when it radiates outwards. The longest path, L_1, is parallel to the earth's sea level. According to the Pythagorean theorem:

$$L_1 = \sqrt{(r_{\text{earth}} + l_1)^2 - r_{\text{earth}}^2} = \sqrt{2 \times r_{earth} \times l_1 + l_1^2} \tag{2}$$

where r_{earth} is the radius of the earth, m; l_1 is the shortest length through the atmosphere to outer space, i.e., the height of the atmosphere. The atmosphere's thickness is approximately 1000 km and the earth's radius is 6371 km, so L_1 is 3707 km.

On the contrary, when the emitter emits thermal radiation in the concentrated RC system, the radiation direction is limited within the half-acceptance angle range of the concentrator, which is showed in Fig. 3(b). The length of the longest path, L_2, needs to be calculated using the Cosine rule:

$$L_2 = \frac{-[2 \times r_{\text{earth}} \times \cos(180^\circ - \theta)] + \sqrt{[2 \times r_{\text{earth}} \times \cos(180^\circ - \theta)]^2 - 4l_2^2 - 8 \times l_2 \times r_{\text{earth}}}}{2} \tag{3}$$

Where l_2 is the same as the thickness of the atmosphere, and θ is the half-acceptance angle of the CPC (30° in this study). Hence, the length of L_2 is about 1129 km, which is much smaller than the longest path of the flat emitter, L_1. Although the relationship between atmospheric thickness and atmospheric transmittance is nonlinear due to variations in air density and water vapor content at different altitudes, i.e., L_2 being one-third of L_1 does not necessarily result in a threefold increase in

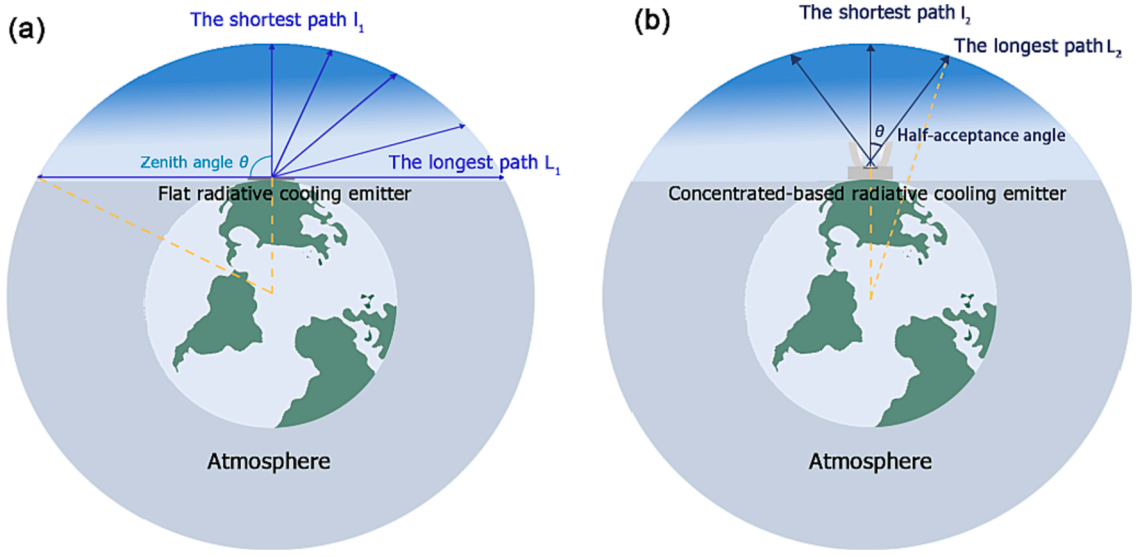

Fig. 3. (a) and (b) Schematic diagram of the radiation path through the atmosphere. The radius of the earth, thickness of the atmospheric layer, and size of the CPC are indicative.

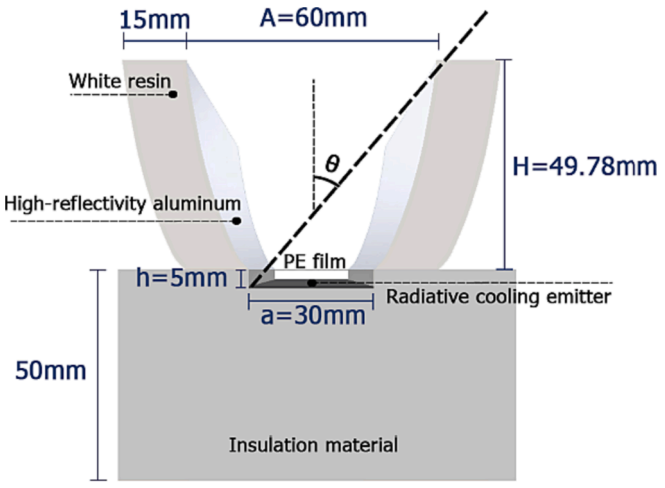

Fig. 4. Schematic cross-section view of the experimental CPC-RC module.

atmospheric transmittance, it is certain that longer thermal radiation paths are associated with lower spectral, directional atmospheric transmittance.

2.2. Experimental design

The schematic cross-section view of the experimental CPC-RC module is depicted in Fig. 4. The CPC-RC module consists of two CPC-shaped reflectors, a transparent polyethene (PE) film, an RC emitter, and a thermal insulation layer. The reflectors are two symmetrical paraboloids, each 15 mm thick, covered with 0.3 mm aluminum mirrors with extremely high reflectivity in the range of 0.3–25 μm (see Fig. 5). The total length of the reflectors is 200 mm. The entrance aperture (A) has a width of 60 mm, while the exit aperture (a) has a width of 30 mm. Based on the theoretical concentration ratio of the CPC as described in Eq. (4) [31], the CPC has a concentration ratio of 2×, and the maximum half-acceptance angle (θ) is 30°.

$$C = A/a = 1/sin\theta \tag{4}$$

To minimize convective heat transfer between the radiative emitter and ambient air, a 15 μm thick polyethylene (PE) film is placed 5 mm above the emitter, creating an air gap. The PE film exhibits high transmittance (around 0.9) in the range of 0.2–25 μm. For the experiment, a hybrid metamaterial-covered RC emitter formed by a 0.4 mm thick aluminum plate and metamaterial is selected [34]. Fig. 5 illustrates the spectral properties of this RC emitter and another black-painted RC emitter as a comparison group in subsection 3.1. The black-painted RC emitter exhibits a weighted average solar absorptivity of 0.66, while the metamaterial-covered RC emitter has a significantly lower weighted average solar absorptivity of 0.13. However, both materials exhibit a high weighted average emissivity of 0.94 in the "atmospheric window", indicating their strong thermal radiation capacity. To minimize cooling losses on the backside of the emitter, a 45 mm thick foam insulation layer is placed at the bottom.

Fig. 6(a) shows the different thermal radiation received and emitted by the horizontally placed CPC-RC module in the outdoor environment. In addition to concentrating the thermal radiation emitted by the emitter, the CPC also serves as a shield against certain solar radiation and atmospheric and surrounding thermal radiation from large incident angles. As depicted in Fig. 6(b) and (c), only downward solar irradiation (P_{solar}), atmospheric thermal radiation (P_{atm}) and surrounding thermal radiation (P_{sur}) that enter the CPC aperture within a θ incident angle (the yellow area), can ultimately reach the emitter surface in a horizontally placed system, with the exception of a small portion entering through the side openings.

Fig. 7 depicts the experimental setup of the system. The experimental system comprises several key components, including different RC modules, K-type thermocouples, a thermocouple shelter, a weather station, a pyranometer, a data logger, and a computer. The K-type thermocouples, calibrated by a high-precision mercury thermometer with an uncertainty of only ±0.05 °C, are positioned at the center of the backside of the RC emitters to record the emitter temperature. Additionally, another thermocouple, protected by the thermocouple shelter, is placed separately to measure the ambient temperature. The weather station records weather parameters such as wind speed and relative humidity. The pyranometer is utilized to measure the solar irradiation on the plane where the module is situated. The test and monitoring devices, along with their uncertainties, are listed in Table 1.

2.3. Solar radiation-related simulation model

The CPC could be a double-edged sword for the cooling performance of the RC emitter during the daytime, depending on whether it blocks or concentrates more solar radiation for the emitter in a specific scenario. As previously discussed, when the solar incident angle is greater than the CPC's half-acceptance angle, the CPC acts as a solar shield which contributes to RC performance enhancement. Otherwise, the CPC becomes a solar concentrator which deteriorates the RC performance. Therefore, this study employs the ray tracing simulation software Photopia [35] to

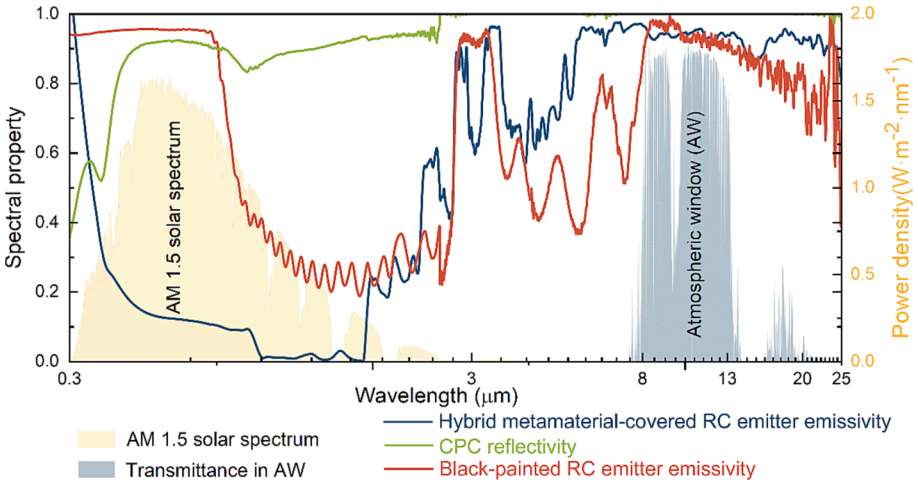

Fig. 5. Spectral characteristics of the metamaterial-covered emitter, black-painted emitter, and CPC surface. The reason for the CPC reflectivity exceeding 1 after 3 μm in the graph is that the measured reflectivity of the CPC surface by the Fourier Transform Infrared Spectrometer surpassed that of the reference material.

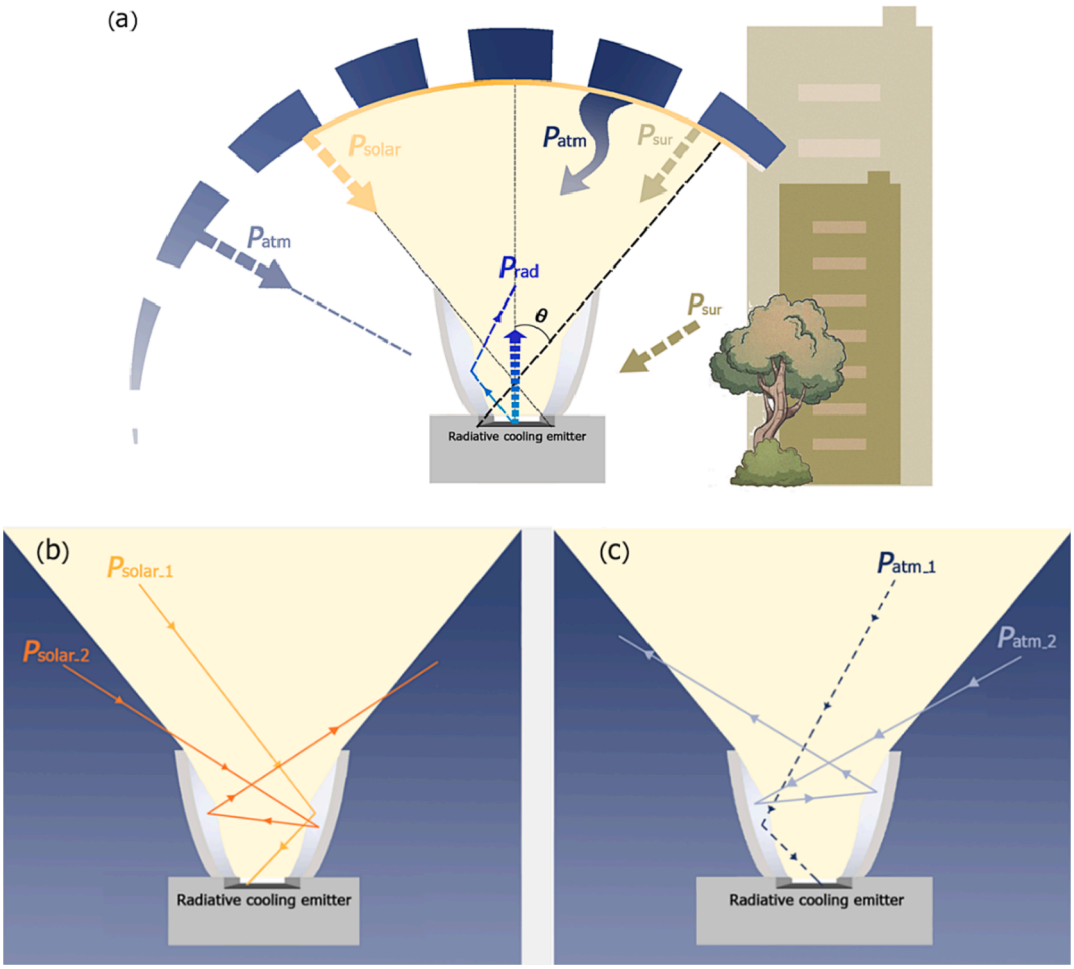

Fig. 6. (a) Different thermal radiation received and emitted by the CPC-RC module. (b) Solar radiation paths at different incidence angles. (c) Atmospheric radiation paths at different incidence angles.

quantitatively exam the effect of the CPC on the solar irradiance absorbed by the RC emitter in various cases (different emitter inclination angles and orientations, different dates). Photopia is a fast and accurate optical design program widely utilized for evaluating complex non-imaging optical systems [36,37]. It offers a wide range of commercially available lamps and includes sun and sky models based on the IESNA RP-21 standard, enabling the simulation of realistic outdoor daylighting conditions.

In the simulation, it is necessary to determine the position of the sun to simulate real illumination. The solar coordinates $(-\cos\theta_h\cos\gamma,\ \cos\theta_h\sin\gamma,\ \sin\theta_h)$ at different times are determined according to the method proposed by Xu Yu et al. [38], where θ_h represents the solar altitude angle, and γ denotes the solar azimuth angle. These values are all calculated by the online calculator [39]. Besides, the reflectors of the CPC-RC module are assigned by specular aluminum with a reflectance of 95 %. Finally, the solar radiation absorbed by the metamaterial-covered RC emitter and black-painted RC emitter are simulated respectively with different placement conditions.

2.4. Outdoor experiment introduction

To evaluate the effect of CPC in the RC system and explore its potential as an alternative to the fragile PE film for wind shading, the first set of experiments compares the emitter temperature difference between the main modules (CPC-RC and flat-RC modules) with and without PE film. Fig. 8 illustrates the schematic of the experiment.

Another comparative experiment is conducted to investigate whether a CPC offers potential advantages for cooling compared to other commonly used concentrators. This experiment involved three modules: a trapezoidal-RC module, a CPC-RC module, and a flat-RC module without any concentrator. Fig. 9 illustrates the experimental setup for this group, in which the trapezoidal concentrator is designed with identical dimensions in terms of height, length, and width as the CPC, and the trapezoidal concentrator forms an acute angle of 70.35° with the horizontal plane. The concept of the geometric concentration ratio of the trapezoidal concentrator is also the same as that of the CPC [40]. The base angle of the trapezoidal concentrator is determined based on the geometric characteristics of the CPC, resulting in an equivalent geometrical concentration ratio of 2×.

Given that building-integrated RC systems often feature RC modules installed on inclined roofs, a third set of experiments is carried out to assess and compare the cooling performance of the CPC-RC and flat-RC modules at various installation angles. Fig. 10 illustrates the arrangement of the RC modules. The sunward group comprises one CPC-RC module and one flat-RC module positioned at a 30° inclination angle facing due south. The anti-sunward group consists of one CPC-RC module and one flat-RC module positioned at a 30° inclination angle towards due north. Additionally, the comparative experimental group includes one CPC-RC module and one flat-RC module placed horizontally.

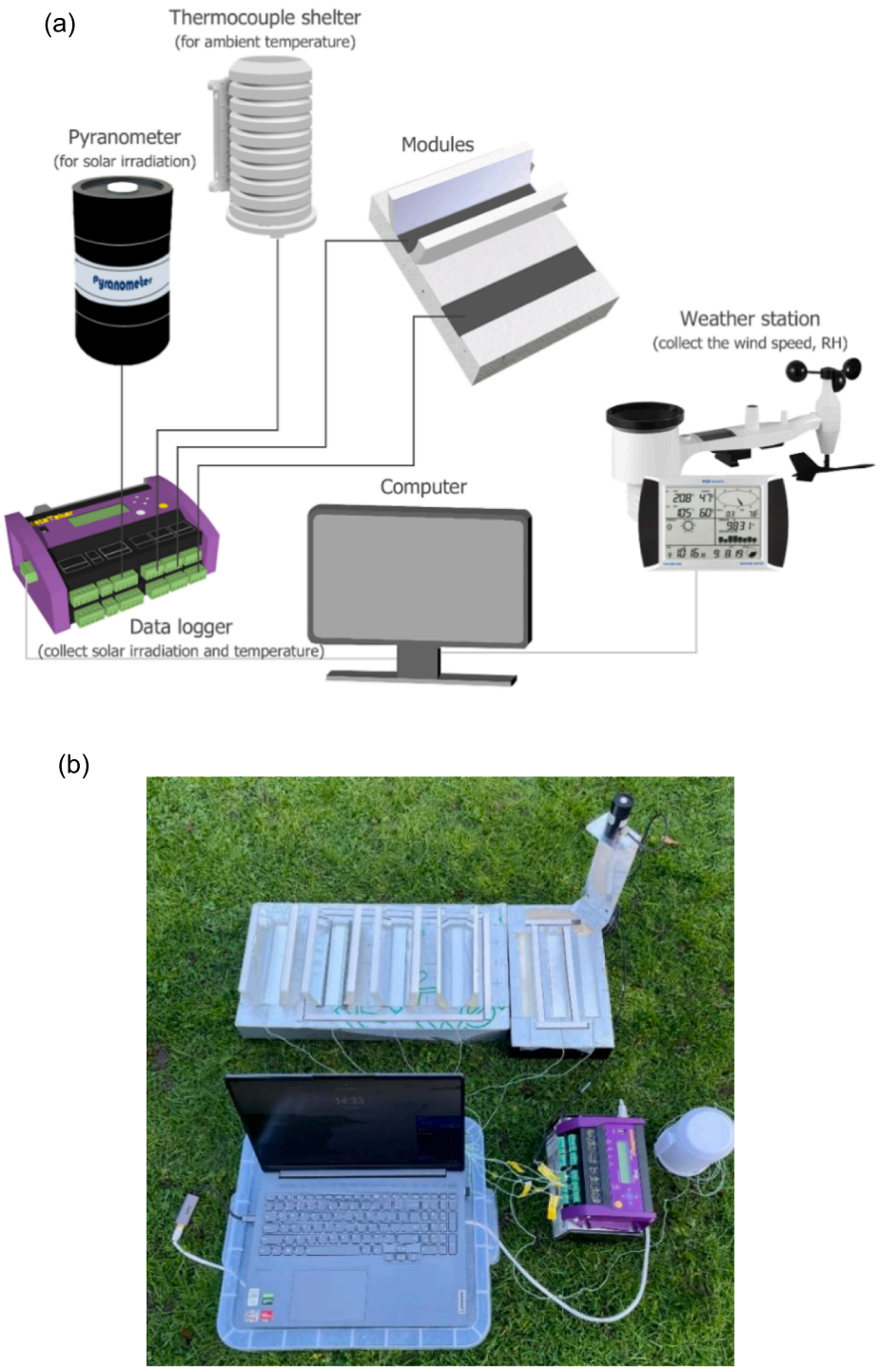

Fig. 7. (a) Schematic of the RC experimental system. (b) In-situ experimental setup of the RC system. The experimental system is located in the open field at the University of Nottingham (52.94°N, 1.09°W), UK with the site altitude being 60 m.

Table 1
List of testing and monitoring devices in the experimental system.

Device	Specification	Uncertainty
Data logger	Data Taker DT80	/
Pyranometer 1	SKL 2650	±2%
Pyranometer 2 and 3	SMP 3	±3%
Thermocouple (calibrated)	Type K	±0.05 °C
Weather station for wind speed	CE-FWS 20N-2	±1 m/s
Weather station for relative humidity	CE-FWS 20N-2	±4% within 20–80 %

3. Results and discussion

3.1. Simulation on the effect of CPC on solar radiation absorption

By utilizing Photopia software, it is possible to analyze the solar radiation absorbed by the RC emitter in both the CPC-RC and the flat-RC modules under various conditions. This analysis enables the identification of scenarios in which the CPC acts as a solar shield or a solar concentrator, resulting in lower or higher solar radiation being absorbed by the emitter compared to the flat-RC module in the same case. For

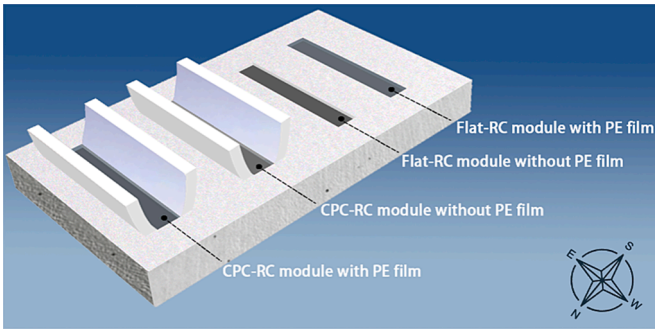

Fig. 8. Experimental setup schematic of the CPC-RC and flat-RC modules with and without PE film.

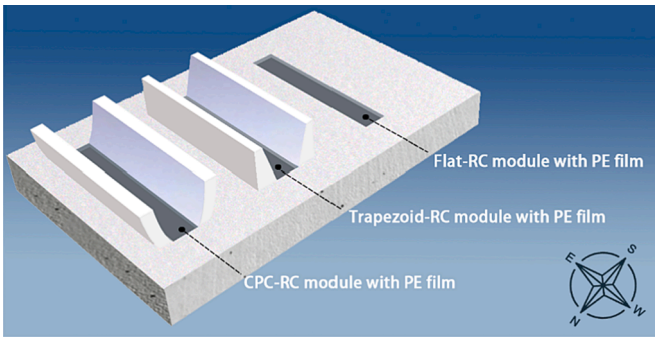

Fig. 9. Experimental setup schematic of three different RC modules.

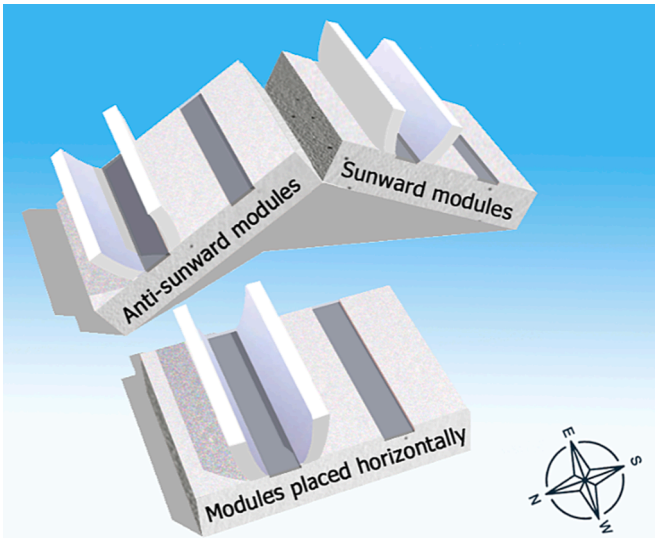

Fig. 10. Experimental setup schematic of three different RC groups under different placements.

accurate modelling in the software, the sizes of the CPC-RC module used in the simulations are kept identical to those of the experimental CPC-RC module detailed in Section 2.2. Similarly, the emitter size for the flat-RC module in the simulation precisely matches that of the experimental flat-RC module.

Fig. 11 displays the solar radiation absorption by CPC-RC and flat-RC modules in Nottingham from June to September, during different placements from 4:00 to 20:00. In Fig. 11(a), both modules show higher solar absorption when tilting 30° to the south, with CPC-RC module exceeding 800 W/m^2 at noon in June and July, 400 W/m^2 more than the flat-RC module. As the month progresses, CPC-RC module's absorption decreases due to higher solar incident angles, transitioning the CPC's function from a concentrator to a shield. In contrast, the flat-RC module maintains steady absorption at around 400 W/m^2. In horizontal placement, the CPC-RC module absorbs more in June and July but less than the flat-RC module in later months. When tilted 30° to the north, the CPC-RC module generally absorbs less than the flat-RC module, except early and late in the day during June and July, due to sunlight entering through the CPC's side openings.

Fig. 11(b) depicts a comparable trend for the metamaterial-covered emitter. Owing to its lower absorptivity in the solar spectrum, this emitter absorbs less solar radiation. The results reveal that except for the side openings of the CPC, when the solar incident angle exceeds the CPC's maximum half-acceptance angle, the CPC effectively acts as a solar shield. This is applicable in scenarios such as when the CPC-RC module is placed horizontally during August and September, or when it is tilted at a 30° angle towards the north. In these cases, the CPC's solar shield effect leads to a lower solar radiation absorption compared to flat-RC modules.

Fig. 12 illustrates the absorbed total solar radiation, summed hourly. Fig. 12(a) shows the total solar radiation absorbed by the black-painted RC emitter. In the south-facing group, the CPC functions as a solar concentrator, leading to significantly higher total solar radiation absorption in the CPC-RC module compared to the flat-RC module during the four typical days. Particularly on June 21st, the total solar radiation absorption value of the CPC-RC module is 6169.78 Wh/m^2, which is 1.64 times that of the flat-RC module. But the gap narrows by September. In the horizontal placement group, the CPC-RC module continues to absorb 1953.62 Wh/m^2 and 462.08 Wh/m^2 higher total solar radiation than the flat-RC module on June 21st and July 21st, respectively. However, the total solar radiation absorbed by it in September is significantly reduced, only one-eighth of that of the flat-RC module. Conversely, For the north-facing group, the flat-RC module consistently absorbs more solar radiation, highlighting CPC's effectiveness as a solar shield. Fig. 12(b) shows the total solar radiation absorbed by the metamaterial-covered RC emitter in different placements over four typical days. The overall trend aligns with Fig. 12(a), which reveals the potential of using metamaterial-covered emitters to enhance the cooling of CPC-RC modules for all-day cooling.

In addition, comparing Fig. 12(a) and (b), in certain cases, even when the CPC-RC module employs a black-painted RC emitter with a lower weighted average emissivity within the solar spectrum, the total solar radiation absorbed throughout the day remains lower than that of the metamaterial-covered flat-RC module. Particularly on September 21st, in the north-facing group, the CPC-RC module with the black-painted RC emitter absorbed a total solar radiation of 48.18 Wh/m^2, significantly smaller than the 110.88 Wh/m^2 absorbed by the metamaterial-covered flat-RC module. This observation further underscores the CPC's effectiveness in providing shading and realizing all-day RC. Consequently, the metamaterial-covered RC emitter is chosen as the emitter for subsequent outdoor experiments.

3.2. Experimental validation of CPC scheme for radiative cooling enhancement

3.2.1. Performance comparison of the CPC-RC and flat-RC modules with and without PE film

In this experiment, the cooling performance of CPC-RC and flat-RC modules with and without PE film was compared to verify the advantage of CPC in RC systems. Fig. 13(a) displays the nocturnal meteorological parameters in Nottingham on May 16th. The ambient temperature exhibited a gradual decrease from 12.29 °C to 7.29 °C during the time span from 21:00 to 23:00. The sky was predominantly clear with minimal cloud cover, and the wind speeds remained relatively low, originating from the east-northeast direction. Significantly, the wind direction aligned almost parallel to the CPC's reflectors, resulting in the wind could through the entire module via the CPC side openings.

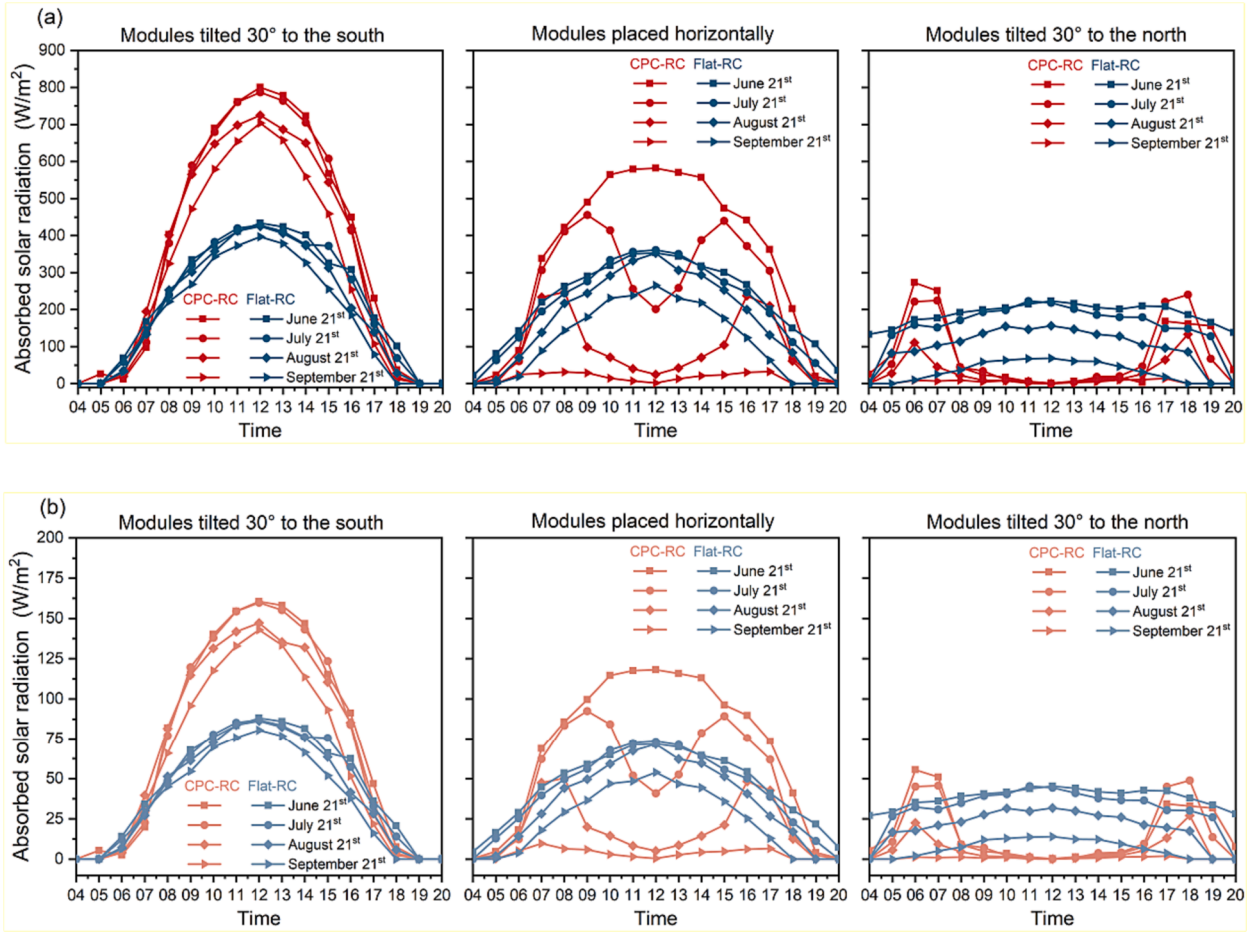

Fig. 11. (a) Solar radiation absorbed by the black-painted RC emitter at three placements on four typical days. (b) Solar radiation absorbed by the metamaterial-covered RC emitter at three placements on four typical days.

When employing a PE film to reduce thermal losses arising from convection and conduction, the CPC-RC module theoretically enhances its cooling capacity by constraining the emitted and absorbed thermal radiation within the half-acceptance angle. As expected, the experimental results depicted in Fig. 13(b) corroborated the significant cooling effect obtained by the CPC-RC module with the PE film. This module consistently maintained the maximum temperature difference compared to the ambient temperature during the entire experimental period. The flat-RC module with PE film ranked second in terms of temperature reduction, demonstrating the effectiveness of RC-coated material in achieving RC at night.

Another objective of this experiment is to investigate the feasibility of utilizing a CPC as a substitute for a PE film to suppress convective heat exchange. The experimental results revealed that the CPC-RC module without the PE film did not achieve the same level of cooling performance as the flat-RC module with a PE film, indicating the CPC's failure in the wind-blocking during this specific test. The effectiveness of the wind-blocking function of the CPC mainly attributes to the wind direction. In cases where the wind velocity component in the length direction of the CPC is dominating, the side openings of the CPC allow wind to enter the module, thereby diminishing the wind-shielding effect, as observed in this experiment. However, it is worth noting that, when the wind velocity component in the length direction of the CPC is minimal or if a CPC without side openings is employed, the CPC may demonstrate potential in replacing the fragile PE film to mitigate convective heat exchange between the RC emitter and ambient air, which requires further experimental demonstration in future studies.

Although this experiment cannot definitively establish the potential of CPC to replace PE film, it highlights CPC's contribution to improving the RC effect. As shown in Fig. 13(b), around 22:20, all modules experienced a certain degree of temperature increase attributable to the presence of thin cloud cover in the sky. This phenomenon is raised from the heightened moisture content introduced by the clouds into the atmosphere, resulting in diminished atmospheric transparency and consequent attenuation of the RC effect. However, the clouds dissipated shortly thereafter, and the temperature of the emitters gradually decreased, albeit at a reduced rate, reaching its lowest point at 23:00. Towards the end of the experiment, the CPC-RC module with PE film achieved the lowest emitter temperature, measured at 1.68 °C. This temperature was 1.55 °C lower than the flat-RC module with PE film and 2.18 °C lower than the CPC-RC module without PE film. The temperature difference (ΔT) between the average emitter temperature and ambient temperature during the experiment is plotted in Fig. 13(c). The CPC-RC module with PE film exhibited the most substantial temperature difference, reaching 5.83 °C, 30 % higher than the emitter temperature reduction observed in the flat-RC module with PE film. These results underscore the considerable potential of combining the CPC and PE film with RC systems to enhance its cooling performance. It has to be acknowledged that, the emitter temperature drop observed in all modules during this experiment is relatively modest compared to the temperature drops reported in other works [41]. This discrepancy can be attributed primarily to the exceptionally humid climate of the test site in the Nottingham area. However, it does not undermine the evidence supporting the positive impact of CPC on enhancing RC performance.

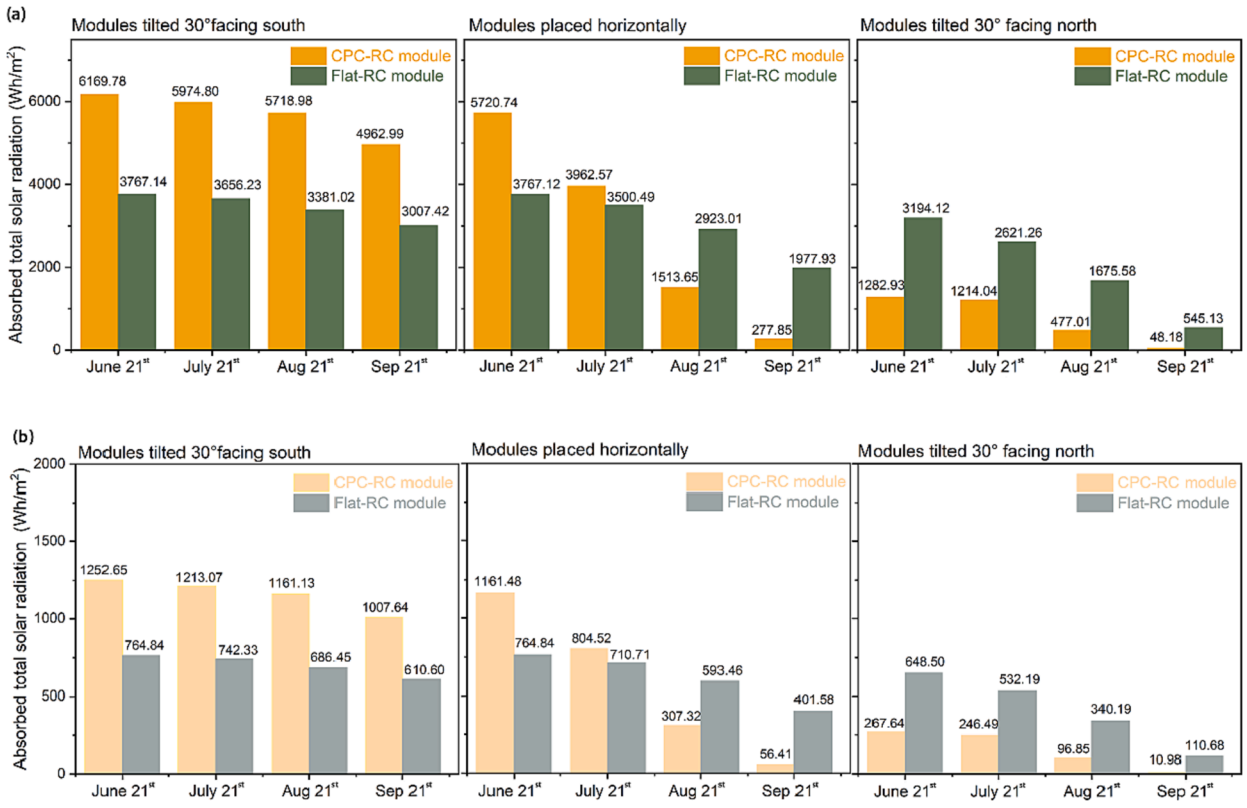

Fig. 12. Total solar radiation absorbed by the CPC-RC and flat-RC modules at three placements on four typical days. (a) Black-painted RC emitter (b) Metamaterial-covered RC emitter.

3.2.2. Performance comparison of the CPC-RC, trapezoidal-RC and flat-RC modules

The second set of experiment compared the cooling performance of three different RC modules, including a CPC-RC module, a trapezoidal-RC module, and a flat-RC module. This experiment was conducted simultaneously with the first set of experiment in Section 3.2.1. A PE film was installed on the top surface of each emitter to minimize the effect of heat convection. Fig. 14(a) illustrated the nocturnal emitter temperature of the three modules. Consistent with the findings of the first experiment, the CPC-RC module exhibited the most significant temperature reduction among the three modules, indicating the high potential of CPC in enhancing RC capabilities. The trapezoidal-RC module, also benefiting from its concentrators, achieved a greater temperature drop compared to the flat-RC module. Nevertheless, despite having the same geometric concentration ratio as the CPC, the trapezoidal-based module exhibited inferior focusing ability due to its lack of a specially designed curved surface that optimizes light concentration. Consequently, its RC performance was lower than that of the CPC-RC module. Fig. 14(b) presented the average temperature difference between the emitter and ambient air. The CPC-RC module demonstrated the most substantial average temperature reduction, reaching 5.83 °C. The trapezoidal-RC module followed closely with an average temperature reduction of 5.13 °C, showcasing an enhancement of 14.5 % compared to the temperature drop observed in the flat-RC module. However, this improvement fell significantly lower than the 30 % enhanced RC effect achieved by the CPC-RC module.

3.2.3. Performance comparison of the CPC-RC and flat-RC modules with different inclined placements

The shielding function of the CPC-RC system also offers a promising solution to overcome challenges faced in utilizing RC technology as a passive cooling strategy for buildings. Typically, RC systems are installed on the roofs or vertical surfaces of buildings. Installing an RC system on a flat roof can achieve efficient cooling capacity. Conversely, when installed on vertical surfaces or steep roofs, the amount of P_{atm} and P_{sur} reaching the RC emitter surface increases, resulting in reduced cooling capability. However, CPC-RC systems have the ability to block unfavorable radiation from large incident angles. This characteristic presents a potential solution to mitigate the negative impact resulting from tilted installations. Therefore, the objective of the third experiment is to assess whether the cooling advantages offered by the CPC-RC module can compensate for the inhibitory effects associated with tilted placements. This will be accomplished by analyzing the temperature variations of both the CPC-RC module and the flat-RC module under various placement conditions. Additionally, the experiment aims to investigate the potential of a north-facing, tilted CPC-RC module in achieving effective RC throughout the day.

This experiment was conducted during two distinct periods: a clear night on May 2nd and a nearly cloudless day on May 24th. Fig. 15(a) illustrates the weather conditions during the nocturnal experiment. From 21:30 to 23:00, the ambient temperature gradually declined from 9.50 °C to 6.97 °C. During the first hour, a gentle breeze was present, but it had mostly subsided by 22:30, and the relative humidity remained constant at 84 % to 89 %. Due to the geographical conditions, there are a few trees and buildings surrounding the north-facing tilted group, while the south-facing tilted, and horizontally placed module enjoy a more open view of the sky. These variables may contribute to minor variations in the results.

Fig. 15(b) shows the emitter temperature of six RC modules with three different placements. It is evident that the temperature variations among the emitters in all six modules followed similar trends. Among these modules, the CPC-RC module placed horizontally exhibited the lowest emitter temperature, whereas the flat-RC module facing north recorded the highest emitter temperature. Fig. 15(c) showed the average temperature difference between the emitters and ambient air. In the horizontal placement group, the CPC-RC module achieved optimal

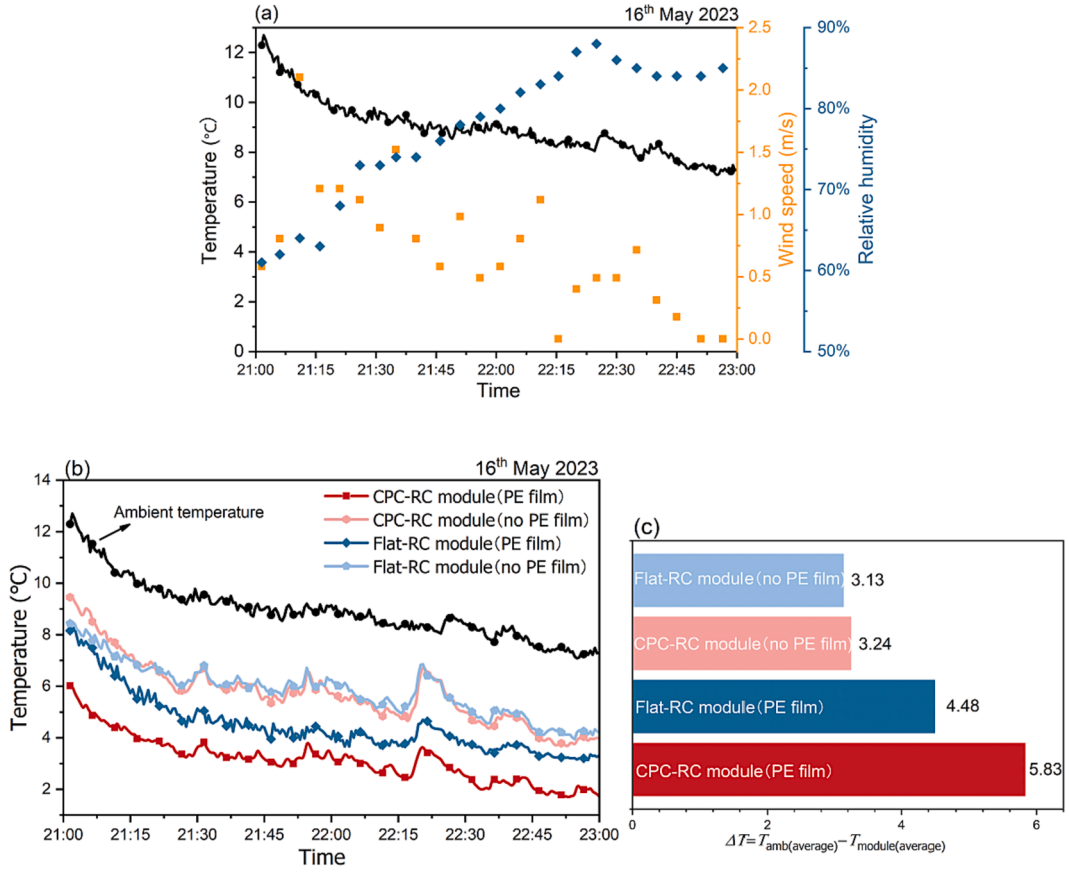

Fig. 13. (a) Weather data in Nottingham, UK on May 16th, 2023. (b) Measured emitter temperatures of the CPC-RC and flat-RC modules with or without PE film. (c) Average temperature differences (ΔT) between the ambient air and emitters.

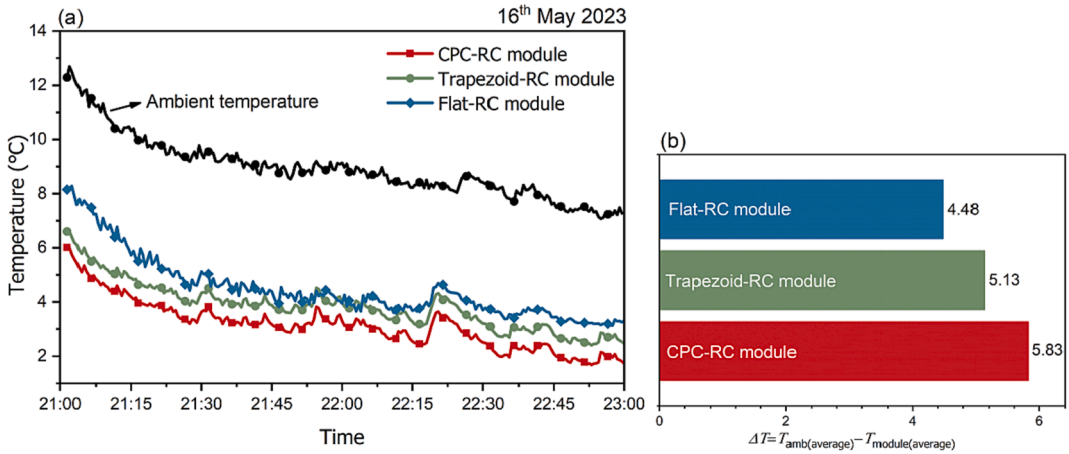

Fig. 14. (a) Measured emitter temperatures of the CPC-RC, trapezoidal-RC and flat-RC modules. (b) Average temperature difference (ΔT) between the ambient air and emitters.

cooling performance, with a temperature drop surpassing that of the flat-RC module by 0.62 °C.

The cooling efficiency of the south-facing group modules was comparatively lower than that of the CPC-RC module in the horizontal placement group. Especially the flat-RC module had worse cooling performance than the same module of the horizontal placement group. This is attributed to the increased zenith angle, leading to thermal radiation needing to pass through the atmosphere with low atmospheric transmittance to reach the outer. Additionally, an emitter placed at an angle experiences a reduced sky view factor, part of it exchanges heat with the warmer surroundings (e.g., the ground, trees, and buildings) rather than with the cooler sky. However, the adverse effects caused by the oblique placement can be compensated for by the CPC scheme, which was clearly demonstrated by the fact that the emitter temperature of the CPC-RC module in the south-facing group was even 0.21 °C lower than that of the flat-RC module in the horizontal placement group.

Both modules in the north-facing group exhibited lower cooling performance during the experiment. This phenomenon was due to the obstruction caused by trees and buildings, blocking the thermal radiation emitted by the emitters from reaching outer space, while also

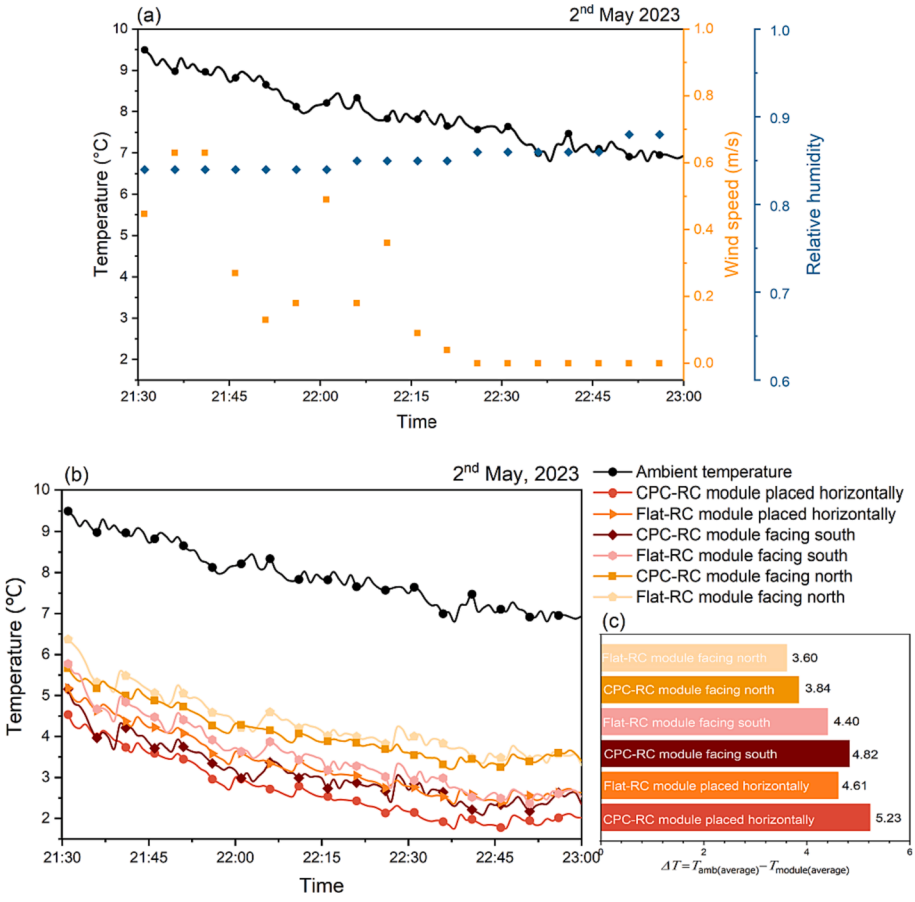

Fig. 15. (a) Weather data in Nottingham, UK on May 2nd, 2023. (b) Measured emitter temperatures of the three placements. (c) Average temperature differences (ΔT) between the ambient air and emitters.

causing the emitters to absorb thermal radiation from the trees and buildings. Nevertheless, the emitter temperature of the CPC-RC module was still 0.24 °C lower than that of the flat-RC module.

Fig. 16(a) depicted the weather conditions during the diurnal experiment. There were light and consistent wind speeds ranging from 0.25 m/s to 1.5 m/s, while the relative humidity remained relatively stable within the range of 40 % to 60 %. The sunward group recorded the highest solar irradiation, surpassing 1000 W/m^2 around 13:00. The horizontal placement group observed lower solar radiation than the sunward group, peaking at approximately 900 W/m^2. In contrast, the anti-sunward group recorded the lowest solar irradiance (the highest value was less than 545 W/m^2).

The emitter temperature of the six modules across the three systems were depicted in Fig. 16(b), alongside the ambient temperature. The figure clearly illustrated that the majority of modules failed to reach sub-ambient temperature, except for the CPC-RC module in the anti-sunward group. Fig. 16(c) showed that the average emitter temperature of the CPC-RC module in the anti-sunward group was 1.59 °C lower than the average ambient temperature throughout the experimental period. Although the temperature difference narrowed at noon, it gradually increased over time. This behavior could be thanked to the function of the CPC as a solar shield, effectively impeding a substantial portion of solar radiation from reaching the emitter. In contrast, the flat-RC module in the anti-sunward group exhibits considerably 3.90 °C higher than the ambient temperature. This discrepancy can be attributed to the absence of a CPC as a shading device, resulting in direct exposure to solar irradiation.

With horizontal placement, neither of the modules achieved sub-ambient temperature. Unlike the anti-sunward group, the average temperature of the CPC-RC module in this group was 4.73 °C higher than that of the flat-RC modules, indicating that the CPC acted as a solar concentrator rather than a solar shield in this case.

In the sunward group, the solar incident angle was significantly smaller than the half-acceptance angle of the CPC, so the CPC effectively concentrated the sunlight onto the emitter. In addition, the flat-RC module was directly exposed to sunlight, resulting in much higher temperatures for the two modules throughout the experiment compared to the other two groups. As shown in Fig. 16(b) and (c), due to the concentrating effect of the CPC, the emitter temperature of the CPC-RC module exceeded 43.21 °C at noon, with an average temperature of 38.78 °C during the entire experiment, surpassing the flat-RC module in the same group by 3.26 °C and the same module in the horizontal group by 1.07 °C. While this temperature is beneficial for solar energy utilization, it can adversely impact RC performance.

4. Conclusion

This study presents a novel CPC-based radiative cooling (RC) system that utilizes a compound parabolic concentrator (CPC) as the concentrator (CPC-RC module). The function of the CPC on the solar radiation absorbed by the RC emitter is evaluated through optical software simulations, and the cooling advantages of the CPC-RC module are assessed through multiple sets of daytime and nighttime outdoor experiments, as compared to the flat RC system (flat-RC module) and trapezoidal-based RC system (trapezoidal-RC module).

1) The solar radiation-absorbed simulation results indicate that the CPC in the RC system can act as a solar shield or concentrator under different cases. During four typical days, the CPC-RC and flat-RC modules in the south-facing group absorb higher solar radiation. However, when the solar incidence angle exceeds the CPC's half-acceptance angle,

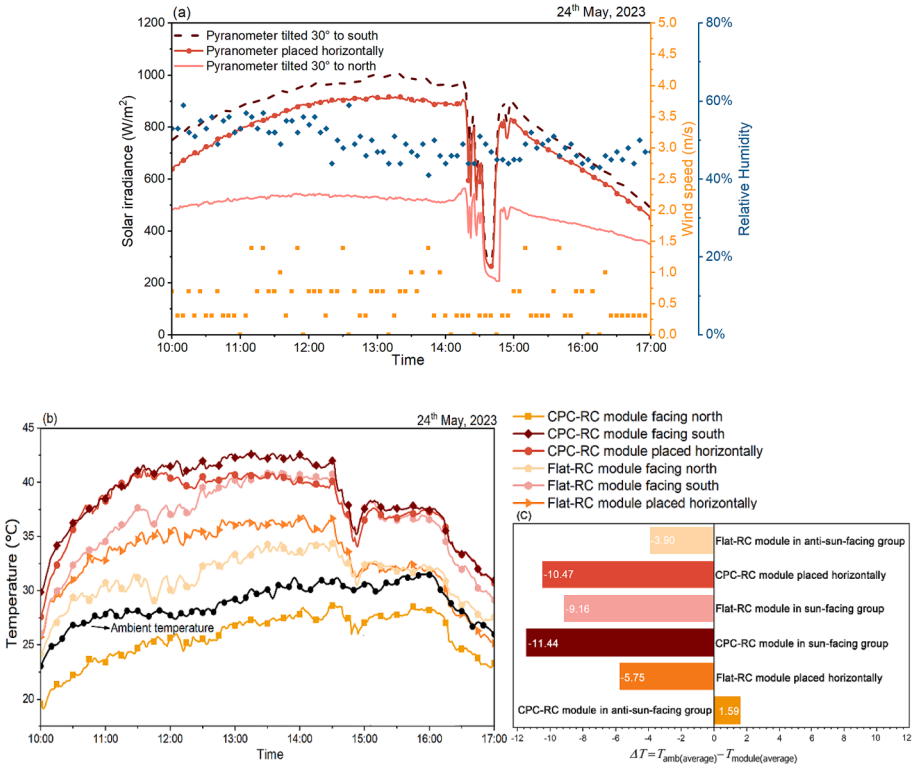

Fig. 16. (a) Weather data in Nottingham, UK on May 24th, 2023, and solar irradiance received by pyranometers in different orientations. (b) The temperature of the 3 groups of systems during the day. (c) Average temperature differences (ΔT) between the ambient air and emitters.

the CPC demonstrates a sun-shading effect. Particularly in the north-facing group, the total solar radiation absorbed by the CPC-RC module with metamaterial-covered emitter was only 267.64 Wh/m^2 on June 21st, about threefold smaller than that of the flat-RC module.

2) The outdoor experiments illustrate the advantages of the CPC in enhancing RC capabilities. By utilizing a polyethylene (PE) film to mitigate the impact of non-radiative heat transfer, the horizontally placed CPC-RC module achieves a temperature of 5.83 °C lower than the ambient temperature at night. This is 30 % higher than the cooling capacity of the flat-RC module and 13.6 % higher than that of the trapezoidal-RC module.

3) The outdoor experiments also demonstrate the influence of wind direction on the wind-blocking effect of the CPC. In the experiments, the opening side of CPC is parallel to the wind direction, resulting in a limited wind-shieling effect. Future investigations will involve optimizing the module's orientation or sealing the CPC sides to assess and enhance the wind-blocking function of the CPC.

4) The experiments of RC modules with different inclined placements indicate that only the CPC-RC module in the anti-sunward group can achieve daytime RC. This is attributed to the shading effect of the CPC, leading to an average emitter temperature of 1.59 °C lower than the ambient temperature. However, other CPC-RC and flat-RC modules fail to achieve sub-ambient RC. Particularly the CPC-RC module in the sunward group, due to the concentration property of the CPC, caused the average temperature of the emitter to reach 38.78 °C, which is 11.44 °C higher than the ambient temperature.

Overall, this paper demonstrates the potential of the CPC-based RC system for all-day RC applications, particularly when tilted towards the north. The concentrating and shading properties of the CPC contribute to its superior cooling performance compared to the flat RC system in the nighttime. These findings provide valuable insights for the development of efficient concentrated RC systems for building cooling applications.

CRediT authorship contribution statement

Ya Dan: Formal analysis, Investigation, Software, Writing – original draft, Writing – review & editing. **Mingke Hu:** Conceptualization, Formal analysis, Investigation, Methodology, Supervision, Writing – review & editing. **Suhendri Suhendri:** Formal analysis, Writing – review & editing. **Yuehong Su:** Conceptualization, Funding acquisition, Project administration, Supervision, Writing – review & editing. **Saffa Riffat:** Project administration, Resources, Writing – review & editing.

Declaration of competing interest

The authors declare that they have no known competing financial interests or personal relationships that could have appeared to influence the work reported in this paper.

Data availability

Data will be made available on request.

Acknowledgements

The authors would like to acknowledge the Engineering and Physical Sciences Research Council (Horizon Europe Guarantee grant number: EP/Y016645/1) for the financial support to this research.

References

[1] A. Pirvaram, N. Talebzadeh, S.N. Leung, P.G. O'Brien, Radiative cooling for buildings: A review of techno-enviro-economics and life-cycle assessment methods, Renew. Sustain. Energy Rev. 162 (2022) 112415, https://doi.org/10.1016/j.rser.2022.112415.

[2] Y. Lei, X. Huang, X. Li, C. Feng, Impact of aging, precipitation, and orientation on performance of radiative cooling for building envelope: A field investigation, Energy Build. 279 (2023) 112716, https://doi.org/10.1016/j.enbuild.2022.112716.

[3] 'Cooling - Fuels & Technologies', IEA. Accessed: Nov. 09, 2022. [Online]. Available: https://www.iea.org/fuels-and-technologies/cooling.
[4] S. Suhendri, M. Hu, Y. Su, J. Darkwa, S. Riffat, Performance evaluation of combined solar chimney and radiative cooling ventilation, Build. Environ. 209 (2022) 108686, https://doi.org/10.1016/j.buildenv.2021.108686.
[5] X. Lu, P. Xu, H. Wang, T. Yang, J. Hou, Cooling potential and applications prospects of passive radiative cooling in buildings: The current state-of-the-art, Renew. Sustain. Energy Rev. 65 (2016) 1079–1097, https://doi.org/10.1016/j.rser.2016.07.058.
[6] H. Ju, S. Lei, F. Wang, D. Yang, J. Ou, A. Amirfazli, Daytime radiative cooling performance and building energy consumption simulation of superhydrophobic calcined kaolin/poly(vinylidene fluoride-co-hexafluoropropylene) coatings, Energy Build. 292 (2023) 113184, https://doi.org/10.1016/j.enbuild.2023.113184.
[7] D. Zhao, et al., Radiative sky cooling: Fundamental principles, materials, and applications, Appl. Phys. Rev. 6 (2) (2019) 021306, https://doi.org/10.1063/1.5087281.
[8] A. Ben-Shalom, B. Barzilai, D. Cabib, A.D. Devir, S.G. Lipson, U.P. Oppenheim, Sky radiance at wavelengths between 7 and 14 μm: measurement, calculation, and comparison with lowtran-4 predictions, Appl. Opt. 19 (6) (1980) 838–839, https://doi.org/10.1364/AO.19.000838.
[9] C.G. Granqvist, A. Hjortsberg, Surfaces for radiative cooling: Silicon monoxide films on aluminum, Appl. Phys. Lett. 36 (2) (1980) 139–141, https://doi.org/10.1063/1.91406.
[10] K. Lin, et al., Nanoparticle-polymer hybrid dual-layer coating with broadband solar reflection for high-performance daytime passive radiative cooling, Energy Build. 276 (2022) 112507, https://doi.org/10.1016/j.enbuild.2022.112507.
[11] A.P. Raman, M.A. Anoma, L. Zhu, E. Rephaeli, S. Fan, Passive radiative cooling below ambient air temperature under direct sunlight, Nature 515 (7528) (2014) 540–544, https://doi.org/10.1038/nature13883.
[12] J. Huang, C. Lin, Y. Li, B. Huang, Effects of humidity, aerosol, and cloud on subambient radiative cooling, Int. J. Heat Mass Transf. 186 (2022) 122438, https://doi.org/10.1016/j.ijheatmasstransfer.2021.122438.
[13] L. Zhou, et al., A polydimethylsiloxane-coated metal structure for all-day radiative cooling, Nat. Sustain. 2 (8) (2019) 718–724, https://doi.org/10.1038/s41893-019-0348-5.
[14] C.N. Awanou, Clear sky emissivity as a function of the zenith direction, Renew. Energy 13 (2) (1998) 227–248, https://doi.org/10.1016/S0960-1481(97)00070-0.
[15] Y. Zhai, et al., Scalable-manufactured randomized glass-polymer hybrid metamaterial for daytime radiative cooling, Science 355 (6329) (2017) 1062–1066, https://doi.org/10.1126/science.aai7899.
[16] S. Zhang, J. Niu, Cooling performance of nocturnal radiative cooling combined with microencapsulated phase change material (MPCM) slurry storage, Energy Build. 54 (2012) 122–130, https://doi.org/10.1016/j.enbuild.2012.07.041.
[17] T. Li, et al., A radiative cooling structural material, Science 364 (6442) (2019) 760–763, https://doi.org/10.1126/science.aau9101.
[18] A. Leroy, et al., High-performance subambient radiative cooling enabled by optically selective and thermally insulating polyethylene aerogel, Sci. Adv. 5 (10) (2019) eaat9480, https://doi.org/10.1126/sciadv.aat9480.
[19] E. Mu, et al., A novel self-powering ultrathin TEG device based on micro/nano emitter for radiative cooling, Nano Energy 55 (2019) 494–500, https://doi.org/10.1016/j.nanoen.2018.10.057.
[20] Y. Wu, et al., Temperature-adaptive porous polymer radiative cooling coatings for all-season thermal management and annual energy-saving, Energy Build. 296 (2023) 113423, https://doi.org/10.1016/j.enbuild.2023.113423.
[21] J. Peoples, et al., Concentrated radiative cooling, Appl. Energy 310 (2022) 118368, https://doi.org/10.1016/j.apenergy.2021.118368.
[22] E.du.M. van Voorthuysen, R. Roes, Blue sky cooling for parabolic trough plants, Energy Procedia 49 (2014) 71–79, https://doi.org/10.1016/j.egypro.2014.03.008.
[23] A.F.G. Jacobs, B.G. Heusinkveld, S.M. Berkowicz, Passive dew collection in a grassland area, The Netherlands, Atmospheric Res. 87 (3–4) (2008) 377–385, https://doi.org/10.1016/j.atmosres.2007.06.007.
[24] 'Exploiting radiative cooling for uninterrupted 24-hour water harvesting from the atmosphere'. Accessed: Nov. 21, 2022. [Online]. Available: https://www.science.org/doi/10.1126/sciadv.abf3978.
[25] Z. Chen, L. Zhu, A. Raman, S. Fan, Radiative cooling to deep sub-freezing temperatures through a 24-h day–night cycle, Nat. Commun. 7 (1) (2016) 13729, https://doi.org/10.1038/ncomms13729.
[26] L. Zhou, et al., Hybrid concentrated radiative cooling and solar heating in a single system, Cell Rep. Phys. Sci. 2 (2) (2021) 100338, https://doi.org/10.1016/j.xcrp.2021.100338.
[27] M. Dong, L. Zhu, B. Jiang, S. Fan, Z. Chen, Concentrated radiative cooling and its constraint from reciprocity, Opt. Express 30 (1) (2022) 275, https://doi.org/10.1364/OE.445544.
[28] A. Gentle, A. Nuhoglu, M. Arnold, G. Smith, *3D printable optical structures for sub-ambient sky cooling*. 2017. doi: 10.1117/12.2274568.
[29] R. Winston, Principles of solar concentrators of a novel design, Sol. Energy 16 (2) (1974) 89–95, https://doi.org/10.1016/0038-092X(74)90004-8.
[30] W.N.A. Wan Roshdan, H. Jarimi, A.H.A. Al-Waeli, O. Ramadan, K. Sopian, Performance enhancement of double pass photovoltaic/thermal solar collector using asymmetric compound parabolic concentrator (PV/T-ACPC) for façade application in different climates, Case Stud. Therm. Eng. 34 (2022) 101998, https://doi.org/10.1016/j.csite.2022.101998.
[31] M. Tian, Y. Su, H. Zheng, G. Pei, G. Li, S. Riffat, A review on the recent research progress in the compound parabolic concentrator (CPC) for solar energy applications, Renew. Sustain. Energy Rev. 82 (2018) 1272–1296, https://doi.org/10.1016/j.rser.2017.09.050.
[32] G. Li, Design and development of a lens-walled compound parabolic concentrator-A review, J. Therm. Sci. 28 (1) (2019) 17–29, https://doi.org/10.1007/s11630-019-1083-3.
[33] C.G. Granqvist, A. Hjortsberg, Radiative cooling to low temperatures: General considerations and application to selectively emitting SiO films, J. Appl. Phys. 52 (6) (1981) 4205–4220, https://doi.org/10.1063/1.329270.
[34] M. Hu, et al., Experimental study on a hybrid solar photothermic and radiative cooling collector equipped with a rotatable absorber/emitter plate, Appl. Energy 306 (2022) 118096, https://doi.org/10.1016/j.apenergy.2021.118096.
[35] 'Optical Design Software | Photopia | Photopia Optical Design Software'. Accessed: Jan. 31, 2023. [Online]. Available: https://www.ltioptics.com/en/optical-design-software-photopia.html.
[36] S. Wittkopf, et al., Ray tracing study for non-imaging daylight collectors, Sol. Energy 84 (6) (2010) 986–996, https://doi.org/10.1016/j.solener.2010.03.008.
[37] M. Tian, Y. Su, Multiple nonlinear regression model for predicting the optical performances of dielectric crossed compound parabolic concentrator (dCCPC), Sol. Energy 159 (2018) 212–225, https://doi.org/10.1016/j.solener.2017.10.090.
[38] X. Yu, Y. Su, A discussion of inner south projection angle for performance analysis of dielectric compound parabolic concentrator, Sol. Energy 113 (2015) 101–113, https://doi.org/10.1016/j.solener.2014.12.024.
[39] 'solar elevation angle (for a day) Calculator', High accuracy calculation for life or science. Accessed: Jan. 31, 2023. [Online]. Available: https://keisan.casio.com/exec/system/1224682277.
[40] M. Alnajideen, M. Gao, A new configuration of V-trough concentrator for achieving improved concentration ratio of >3.0x, Sol. Energy Mater. Sol. Cells 245 (2022) 111877, https://doi.org/10.1016/j.solmat.2022.111877.
[41] M. Hu, et al., Applications of radiative sky cooling in solar energy systems: Progress, challenges, and prospects, Renew. Sustain. Energy Rev. 160 (2022) 112304, https://doi.org/10.1016/j.rser.2022.112304.